Numerical Modeling of a Coastal Trapped Disturbance. Part II: Structure and Dynamics

PETER L. JACKSON

Environmental Studies Program, University of Northern British Columbia, Prince George, British Columbia, Canada

CHRIS J. C. REASON

School of Earth Sciences, University of Melbourne, Melbourne, Australia

SHUCAI GUAN

Environmental Studies Program, University of Northern British Columbia, Prince George, British Columbia, Canada

(Manuscript received 25 October 1997, in final form 5 May 1998)

ABSTRACT

A detailed analysis of a simulation of a coastal trapped disturbance (CTD) using the Colorado State University Regional Atmospheric Modeling System (RAMS) is presented. The CTD considered (15–18 May 1985) represents an example of a strong mesoscale trapped event with abrupt gravity current–like transitions in many meteorological parameters, and which was closely tied to the synoptic forcing. Propagation of this event along the west coast of North America occurred from initiation in the Southern California Bight–Baja California coastal region to the northern tip of Vancouver Island, and the event appeared to have no difficulty in negotiating significant bends or gaps in the coastal mountains unlike some other events that have ceased or stalled near Cape Mendocino, Point Arena, and the mouth of the Columbia River.

It is found that warm offshore flow ahead of the CTD, and cool onshore flow in the Southern California Bight–northern Baja California coastal region, both driven by the westward tracking of a synoptic low, are very important for initiation, and subsequent propagation, of the model CTD, similar to observations. Convergence of the initial onshore cool flow in the south combined with warm offshore flow in the north lead to a northward-directed pressure gradient and, hence, a southerly wind transition. The adjustment timescale of the onshore flow to form the southerlies of the CTD is found to be consistent with expectations from theory.

During the propagating stage of the event, the pressure gradient and Coriolis terms were found to be most important for the meridional wind tendency, with advection and diffusion making smaller contributions. Consistent with semigeostrophic theory for CTD, the length scale in the across-mountain direction of the model CTD is much less than the along-mountain scale. Although the model transitions in winds, pressure, and temperature are not as sharp as observed (attributed to the lack of boundary layer structure in the NCEP fields used for model initialization), there is some signature of the gravity current nature of the event.

Decay of the event occurred when the favorable synoptic forcing related to the synoptic low moved to the northwest. There appeared to be no evidence of any topographic influence on the decay or termination of this particular event, unlike for several other cases.

Taken together, this and the previous validation study suggest that RAMS can be usefully employed to better understand the nature of at least these strong CTD events.

1. Introduction

Coastal trapped disturbances (hereafter CTDs) are mesoscale systems that are laterally confined against a coastal mountain barrier by Coriolis effects and vertically confined by stable stratification. CTDs propagate along the coastal mountain barrier such that the barrier is on the right (left) in the Northern (Southern) Hemisphere. Propagation is generally energetic but relatively short lived (typically 2–3 days on the North American west coast). Typical length scales are 1000 km alongshore, 100 km across-shore, and 0.5 km in the vertical (Reason 1994). CTDs along the west coast of North America are generally coastal ridges of higher pressure in the marine layer and result in a wind reversal from the typical northerly to southerly flow (e.g., Dorman 1985, 1987; Mass and Albright 1987; Reason and Dunkley 1993).

The CTD of 15–17 May 1985 along the west coast

Corresponding author address: Dr. Peter L. Jackson, Environmental Studies Program, University of Northern British Columbia, 3333 University Way, Prince George, BC V2N 4Z9, Canada.
E-mail: peterj@unbc.ca

of North America, documented by Mass and Albright (1987, hereafter MA87), represents an example of a strong mesoscale trapped event with abrupt transitions in many basic meteorological parameters, and which appeared to be closely tied to the synoptic forcing. Validation of a simulation of this particular event using the Colorado State University Regional Atmospheric Modeling System (RAMS) has been presented in a previous paper (Guan et al. 1998, hereafter GJR98), and details of the model and its configuration can be found there. In this study, the objective is to use more detailed output from RAMS simulations to examine the event's initiation mechanism, the structure of the flow, and to assess the dynamical balance accounting for its propagation and decay characteristics in the presence of complex coastal orography.

2. CTD initiation

a. Synoptic aspects

In GJR98, it was found that southerly winds near the coast (the CTD) were initiated south of that simulation's grid 2 domain (25-km horizontal resolution), and so a detailed examination of the initiation mechanisms was not possible. Also, the GJR98 simulation contained a slow nudging toward the National Centers for Environmental Prediction (NCEP) reanalyses in the interior of the coarsest (100-km resolution) of the nested model grids as well as nudging at the boundaries of this grid. In the present study, the run from GJR98 is repeated but with nudging toward the NCEP initial and time-dependent boundary conditions turned off in the interior of the coarse grid and in the entire domain of the nested grids except near the top boundary. This significantly improved the model's boundary layer simulation in spite of the fact that the NCEP analyses used as initial conditions still do not adequately represent the boundary layer. In addition to further analysis of output from this run, the results of an additional simulation are examined here. In the additional simulation, grid 2 extends 12° latitude farther south and 2° longitude farther east than in GJR98 in order to capture the meso- to synoptic-scale situation that leads to the initiation of the disturbance.

Figure 1a shows the simulated sea level pressure and wind fields at 118-m elevation (level 3 in the model) during the initiation of the May 1985 event. At 1600 UTC 15 May, westerly and northwesterly (i.e., essentially, onshore) wind prevailed over the coastal waters of southern California and northern Baja California except very close inshore where light southeasterly flow was initiating. During the next 8 h, the wind shifted to southwesterly in this region. By 0800 UTC 16 May, the nearshore winds were mainly southerly, and the model CTD was under way. Figure 18 of GJR98 indicates that the model timing for the switch to southerlies in the Southern California Bight was perhaps 2–3 h later than the observed, whereas in the current simulation, the model initiation of the CTD is closer in time to the observed.

The model wind field at 850 hPa (Fig. 1c) indicates that southerly winds over the region offshore from southern California and Baja California developed at this level in response to the westward moving synoptic low, simultaneously with those near the surface (e.g., fields at an elevation of 118 m, Fig. 1a), but that the extent of the turning of the wind to southerly is not quite as pronounced as the near-surface flow (cf. near the Point Conception to Monterey coast for 0000 and 0800 UTC 16 May). Associated with the onset of southerlies is the formation of a cold pool, which developed offshore of San Francisco (Fig. 1b at 118 m). The cold pool was associated with a westward propagating synoptic low evident at both 850 and 500 hPa (GJR98) that was initially centered over northern Nevada, and then migrated westward over northern California–southern Oregon and out over the Pacific. At 1300 UTC 16 May the cold pool reached its maximum areal extent, with a near-surface temperature below 7°C.

While the winds in the Southern California Bight were making a transition to southerly, the temperature field along the coast to the north was also adjusting. Figure 2 shows the simulated vertical cross sections of potential temperature along the California and Pacific Northwest coasts during the event and the initiation of southerly flow (in this figure and in Fig. 5 the steep gradients and missing data regions at the northern end of each plot represent where the transect approaches, and intersects, Vancouver Island and the British Columbian mainland to its north). At 1200 UTC 15 May, there was a small south–north potential temperature gradient, with warmer temperature in the south, and cooler temperature in the north. The highest near-surface potential temperature was 286 K near San Francisco and the lowest potential temperature was 278 K near Quillayute. During the next 12 h (through 0000 UTC 16 May) the potential temperature increased in the north and decreased in the south. In the north, offshore flow from the interior in response to the westward tracking synoptic low lead to warm subsiding air, which increased the potential temperature there. The decreased potential temperature in the south resulted in part from movement of the cold pool associated with the synoptic low and onshore flow associated with the circulation around the southern part of the low. By 1200 UTC 16 May, the alongshore temperature gradient had reversed orientation and strengthened with cold air in the south and warm air in the north, representing a significant northward-directed density gradient.

Based on the above, and examination of the meso- and synoptic-scale model fields at various levels in GJR98, it appears that initiation of this particular event was brought about by the westward tracking synoptic low and its associated circulation in the region, which resulted in a northward-directed pressure gradient and, hence, southerly flow, in the coastal zone. The specific

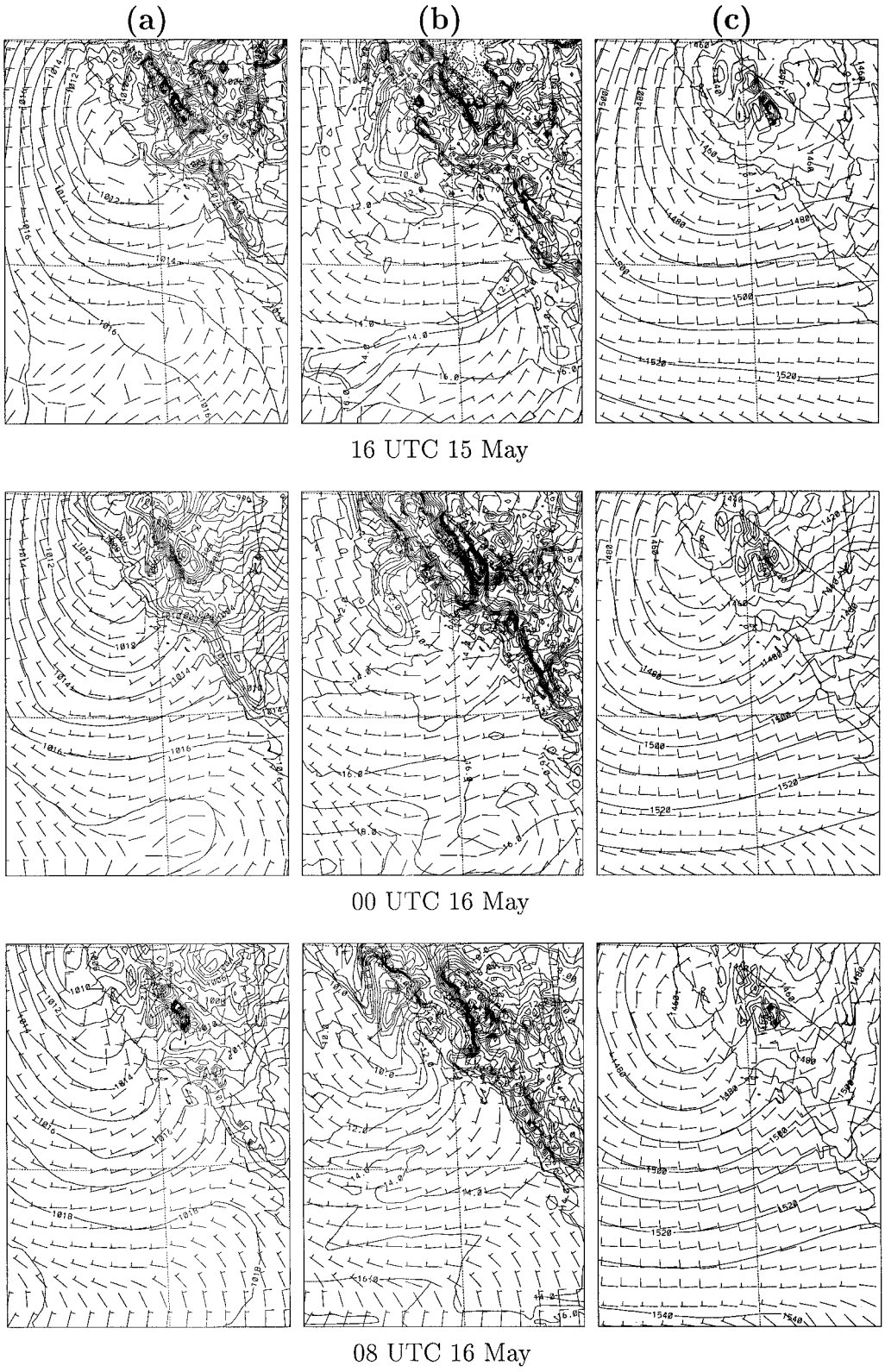

FIG. 1. Simulated grid 2 fields during the initiation of the May 1985 event. (a) Sea level pressure (contour interval 1 mb) and wind fields at 118 m above the surface. (b) Temperature (contour interval 1°C) and wind at 118 m above the surface. (c) Geopotential height (contour interval 10 m) and wind at 850 hPa.

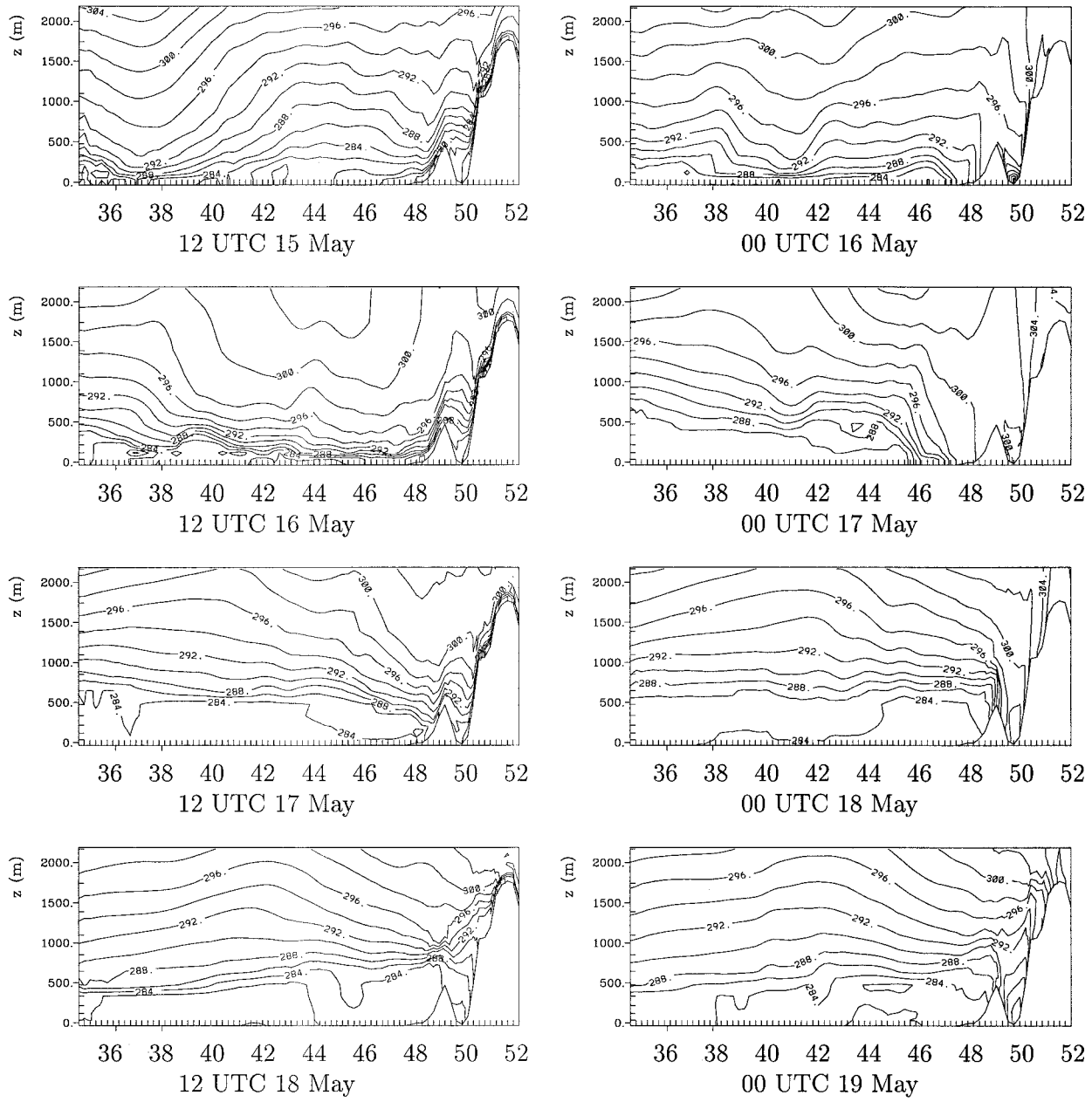

FIG. 2. Simulated south–north vertical cross sections of potential temperature along the California and Pacific Northwest coasts during the May 1985 event from grid 2 of the model. The cross section is located just offshore of the northern California to Washington coasts and extends from offshore of Point Conception in the south to north of Vancouver Island in the north. Numbers along the horizontal axis indicate the latitude. Contour interval is 2 K.

responses in the coastal atmosphere to this synoptic forcing that initiated the CTD were 1) offshore flow to the north resulted in adiabatic and advective warming near the surface there with associated reduction in surface pressure, 2) low-level temperatures offshore from San Francisco cooled with the passage westward of the synoptic low, and 3) onshore flow south of the synoptic low and especially in the Southern California Bight lead to convergence of relatively cool, dense air against the coastal mountains and subsequent adjustment to southerly flow.

b. ''Force balance'' analysis

In order to assess the relative contributions of the various terms that might be important in the generation of the event, the ''force balance'' capability of RAMS can be invoked. Because RAMS produces a dynamically

balanced ''dataset'' at high spatial and temporal resolution, the model can be used to extract the forces that make up the individual components of the momentum equation. These forces act to accelerate or decelerate wind and, hence, account for its spatial and temporal variation during the event.

The RAMS horizontal momentum equation has five terms: 1) total momentum tendency (the acceleration), which is a consequence of the other tendencies or forces (tot); 2) tendency due to pressure gradient force (pgf); 3) tendency due to advection of momentum (adv); 4) tendency due to parameterized subgrid-scale turbulent diffusion (dif); and 5) tendency due to Coriolis acceleration (cor). The abbreviations in parentheses above match those used in the figures discussed next, which illustrate the force balances existing in the model.

Figure 3 displays tendencies of meridional wind at 118-m elevation near the time of initiation: 1600 UTC 15 May. The total positive (i.e., southerly) tendency in the meridional wind offshore in the Southern California Bight shown in Fig. 3a is caused by the large positive tendency due to the pressure gradient force (Fig. 3b), which is only partially offset by the negative tendency of the Coriolis force (Fig. 3e). By comparison, the tendencies of meridional wind due to diffusion and advection in the coastal zone are generally much smaller than either the pressure gradient or Coriolis terms over most of the coastal domain. A narrow zone of large positive advection tendency in the northwest quadrant of the domain (Fig. 3c) is the result of westward advection of decreased northerly momentum associated with the western flank of the synoptic low. Farther offshore, near the western boundary of the model domain, the diffusion tendency (Fig. 3d) becomes significantly positive; this represents the frictional retardation of the strong northerly winds (Fig. 1a) by the sea surface in this location. In the Southern California Bight, the northward-directed pressure gradient tendency dominates, resulting in the transition to southerly winds (i.e., the CTD) there. In the near-coastal zone large positive tendencies due to the Coriolis force are the result of flow with an easterly component there (i.e., offshore flow ahead of the CTD). The tendencies of meridional wind 8 and 16 h later, that is, at 0000 and 0800 UTC 16 May, are mostly similar to those at 1600 UTC 15 May with the pressure gradient and positive total tendencies increasing and moving northward as the initiation of the CTD proceeds (Fig. 4) and the event moves up the coast. At 0000 UTC 16 May, deceleration of now onshore flow results in a Coriolis tendency maximum (Fig. 4c) of $> -2 \times 10^{-4}$ m s^{-2} near the Catalina Islands. By 0800 UTC 16 May, a narrow coastal zone of positive Coriolis tendency results from the CTD flow, which due to the orientation of the coastal mountains, has an easterly component. This feature is discussed more in the next section.

c. Mechanism of CTD initiation

As already mentioned, the westward tracking of a synoptic low from northern California–southern Oregon, with associated offshore flow to the north (i.e., ahead of the CTD) and onshore flow to the south (i.e., in the CTD generation region), which created a northward-directed pressure gradient anomaly along the coast, was important for the initiation of the model CTD. A similar situation occurred during the observed event (MA87). In other words, modulation of the climatological southward-directed pressure gradient along the coast by the tracking synoptic low appears to have been more important than direct pumping of the marine boundary layer in the Southern California Bight for the CTD initiation in this particular case. Detailed examination of model vertical velocity cross sections in the Southern California Bight showed little or no vertical flow during the initiation, and very weak subsidence during the propagation stage.

The adjustment of the onshore flow in the bight during the initiation of the CTD can be understood using the theory of Pierrehumbert and Wyman (1985) as applied to the CTD situation by Reason (1994). In this hydrostatic theory, a Boussinesq stratified zonal flow U upstream of a mesoscale mountain (such as those along the California coast) of half-width L_m and height H_m is expected to be be blocked for times between L_m/U and $1/f$ (minutes to several hours) if the Froude number $\mathrm{Fr} = U/NH_m$ (N is the Brunt–Väisälä frequency) is unity or less. The initial blocking of this upstream flow and associated convergence against the topography leads to the mesoscale coastal high pressure anomaly (the beginnings of the CTD) in the Southern California Bight. On timescale $\geq 1/f$, the blocking of the onshore flow may persist for the small Rossby number case if the ratio of the Rossby to the Froude number $\mathrm{Ro/Fr} = NH_m/fL_m \geq 1$, and for the large Rossby number case if $\mathrm{Fr} \leq 1$. The case where $U/fL_m = \mathrm{Ro} = 1$ is a transition between the two regimes of small and large Rossby number.

Typical scales of observed previous CTD events along the U.S. west coast (Reason 1994) indicate that Fr is small compared to unity, suggesting that the initial onshore flow may be blocked on timescales of minutes to a few hours. These scales also give $\mathrm{Ro} = O(1)$, and hence $\mathrm{Ro/Fr} \geq 1$, suggesting that advective effects may be significant, and that initial blocking may persist beyond a timescale of $1/f$ for CTD events here (Reason 1994). The same scales can be computed for the model CTD event under consideration. From Fig. 1a, a typical onshore wind speed in the Southern California Bight may be taken as 2.5 m s^{-1}. Based on the 10 arc-minute topographic dataset supplied with the RAMS code and used here, $H_m = 1000$ m, and $L_m = 20$ km for the Californian coastal mountains at 32°S (near San Diego). The Brunt–Väisälä frequency N of the model coastal atmosphere near San Diego was computed from the for-

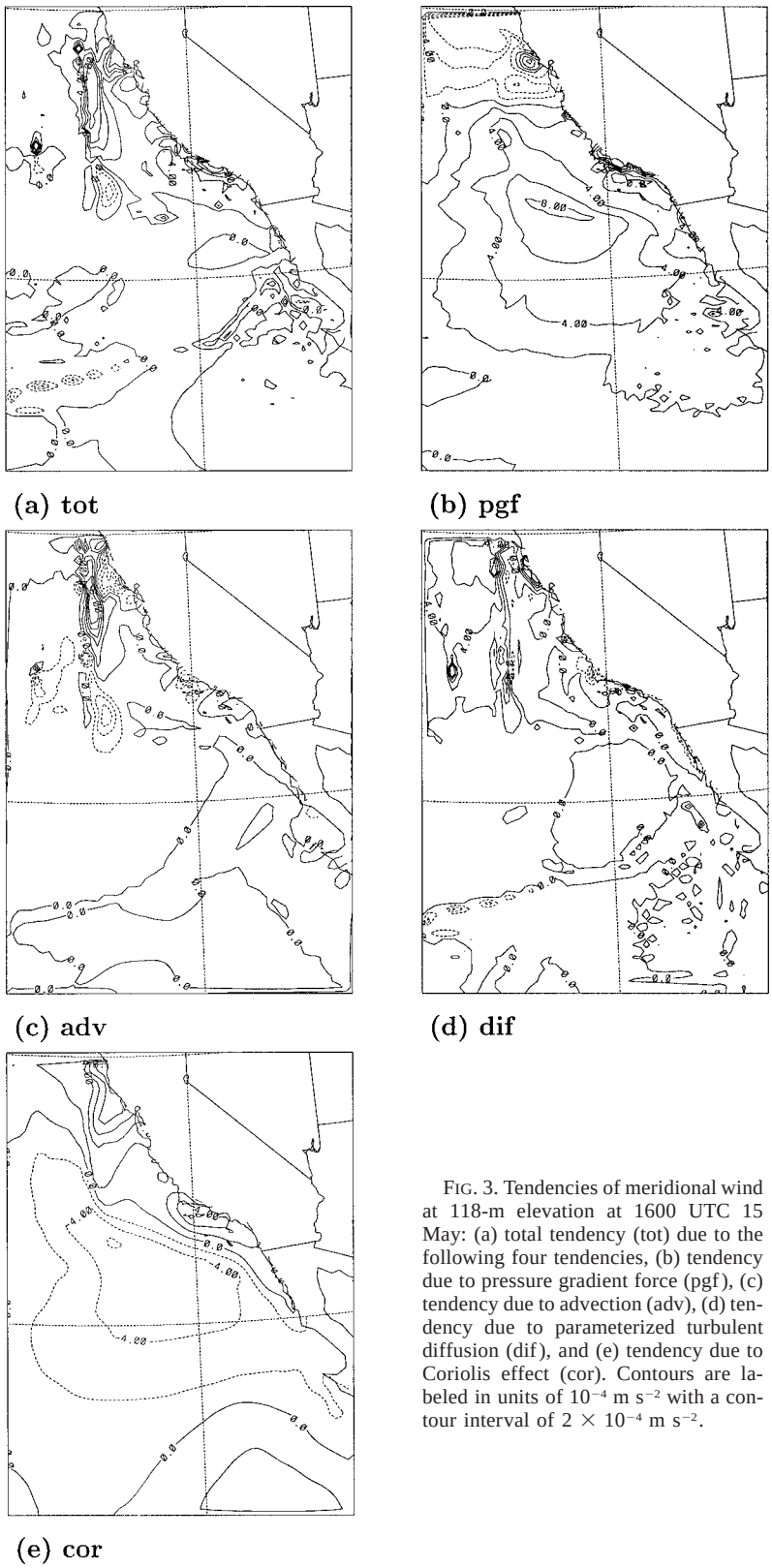

FIG. 3. Tendencies of meridional wind at 118-m elevation at 1600 UTC 15 May: (a) total tendency (tot) due to the following four tendencies, (b) tendency due to pressure gradient force (pgf), (c) tendency due to advection (adv), (d) tendency due to parameterized turbulent diffusion (dif), and (e) tendency due to Coriolis effect (cor). Contours are labeled in units of 10^{-4} m s^{-2} with a contour interval of 2×10^{-4} m s^{-2}.

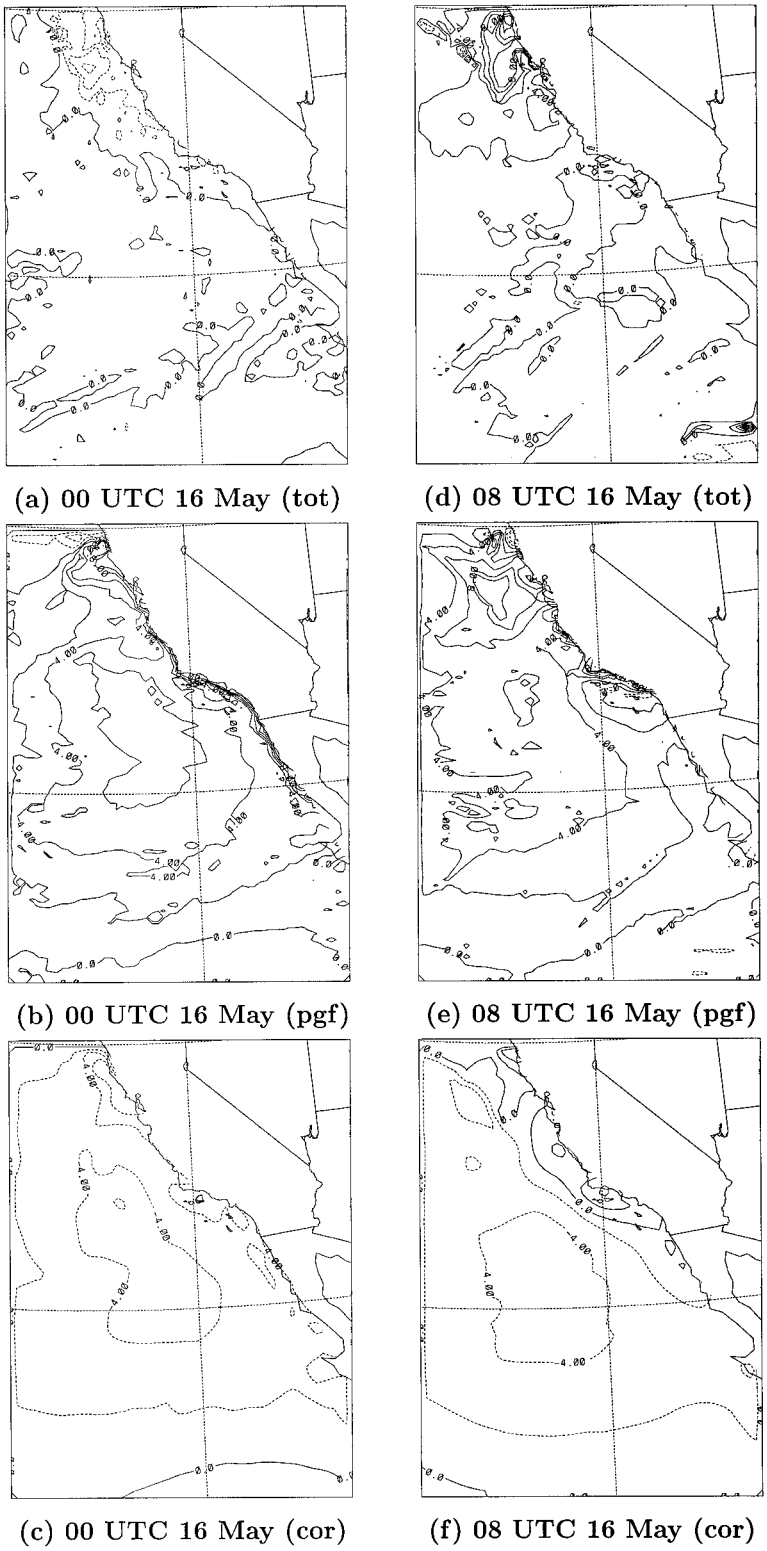

FIG. 4. Tendencies of meridional wind at 118-m elevation: (a) 0000 UTC 16 May tot, (b) 0000 UTC 16 May tendency due to pgf, (c) 0000 UTC 16 May tendency due to cor, (d) 0800 UTC 16 May tot, (e) 0800 UTC 16 May tendency due to pgf, and (f) 0800 UTC 16 May tendency due to cor. Contours are labeled in units of 10^{-4} m s^{-2} with a contour interval of 2×10^{-4} m s^{-2}.

mula $N^2 = (g\Delta\theta)/(\theta\Delta z)$ to be 0.016 s^{-1}. Evaluation of the scales for the model output for 1600 UTC 15 May gives a Froude number of 0.16, which is indeed small compared to unity. Thus, one might expect the initial onshore flow (on timescales of minutes to a few hours) to be blocked by the coastal mountains. The Rossby number based on the mountain half-width is computed as Ro = 1.6 = $O(1)$, similar to the observed event. Thus, Ro/Fr $\geq$ 1, and the blocking of the onshore flow may persist for times greater than $1/f$, or about 3–4 h at the latitude of the Southern California Bight.

As the onshore flow approaches the coastal mountains, it must decelerate. On timescales of order $1/f$, weakening of the Coriolis term fu in the meridional momentum equation will then turn this flow to the left in the Northern Hemisphere, and the generation of this alongshore flow marks the beginning of CTD formation proper (Reason 1994). This argument is supported by the force balance analyses for 0000 and 0800 UTC 16 May (Figs. 4c,f), which shows a maxima in the southerly tendency due to the Coriolis force in a narrow zone along the coast due to deceleration of the onshore flow by the coastal mountains.

Examination of the near-surface model pressure and wind fields (Fig. 1a) for 1600 UTC 15 May to 800 UTC 16 May suggests that the onshore flow present offshore in the Southern California Bight by 1600 UTC 15 May had begun to significantly turn to the left by 0000 UTC 16 May (8 h later), and showed significant southerly flow (the CTD) after a further 8 h (0800 UTC 16 May), consistent with the $1/f$ timescaling. For times after 0800 UTC 16 May, the switch to southerly winds (associated with the arrival of the CTD at a given location) moved farther north along the coast toward Vancouver Island. The dynamics of the CTD during this propagating stage are considered in detail in the next section.

3. Propagation dynamics

After the CTD formed along the coast of southern California and northern Baja California, it propagated northward along the coast as far as northern Vancouver Island. During this process, temperature, wind, and pressure fields along the coast changed rapidly as the CTD passed through a given station.

Figure 2, presenting vertical cross sections of potential temperature during the CTD, is located approximately along 125°W, just offshore of the coast as it is oriented between northern California and the Strait of Juan de Fuca. The cross sections of meridional wind, and coastal sea level pressure variations with latitude (Fig. 5), show the southerly wind transition to have reached San Francisco Bay (about 38°N) by 0600 UTC 16 May, as the northward-directed pressure gradient in the south strengthened. At this stage, the coastal sea level pressure minimum was slightly ahead of the southerly wind transition, as in the observed event (MA87). Offshore flow ahead of the CTD and onshore flow in the south, driven by the synoptic low, resulted in warm potential temperatures and falling pressures near the surface (i.e., above a shallow stable surface layer associated with cool sea surface temperature) along the Oregon and Washington coasts with cool potential temperatures and increasing sea level pressure farther south, particularly in the Southern California Bight (Figs. 2 and 5). In other words, a significant (and strengthening until at least 0000 UTC 17 May) temperature gradient, and hence northward-directed density gradient, existed along the U.S. west coast on 16–17 May leading to the gravity current–like signature of the event in the observations (MA87) and in the model (Figs. 2 and 5).

As discussed in GJR98, the model initialization fields from NCEP do not resolve the marine boundary layer so the model may not optimally represent this layer and, particularly, the steep gravity current–like nature of the leading edge of the CTD. However, once the weak interior nudging of the model grid 1 solution toward NCEP data was turned off, the boundary layer representation and gravity current–like nature of the event became significantly more realistic (Figs. 2 and 5) than in the simulation of GJR98.

Examination of the potential temperature cross sections (Fig. 2) and relative humidity cross sections (now shown) suggests that a gravity current–like feature had evolved in the lowest 1000–1500 m and propagated to near 46°N at the time (0000 UTC 17 May) of maximum northward-directed temperature (density) gradient and sea level pressure gradient (Fig. 5). Ahead of the gravity current feature during the 1200 UTC 15 May to 0000 UTC 17 May period, was a shallow stable layer extending along the coast to Vancouver Island and the British Columbian mainland. Some representation of the greater depth of the gravity current head than the flow behind can be seen in Fig. 2 at 0000 UTC 17 May near, and south of, 44°N, and the stable cool air feeding the gravity current head is evident. Associated with the leading edge of the gravity current–like feature was the transition from northerly winds ahead of the event to the southerlies of the event itself (Fig. 5), the minimum in coastal sea level pressure was still slightly ahead (on the Washington coast) of the wind transition, similar to the observed event (MA87). Figure 5, particularly for the period 1200 UTC 16 May to 0600 UTC 17 May, suggests that the simulated transition from northerly to southerly winds at the leading edge of the CTD is evident first at elevation (i.e., at about 100–500 m) before it is seen at the surface. Data limitations precluded detection of such behavior in the MA87 study; however, observations of a June 1994 event (Ralph et al. 1995) do suggest the wind transition at elevation leading that at the surface.

Twelve to eighteen hours later (1200–1800 UTC 17 May), the leading edge of the gravity current–like feature had reached Vancouver Island at the northern end of the transect, and the feature was deeper than earlier as relatively cool, dense marine air existed all along the

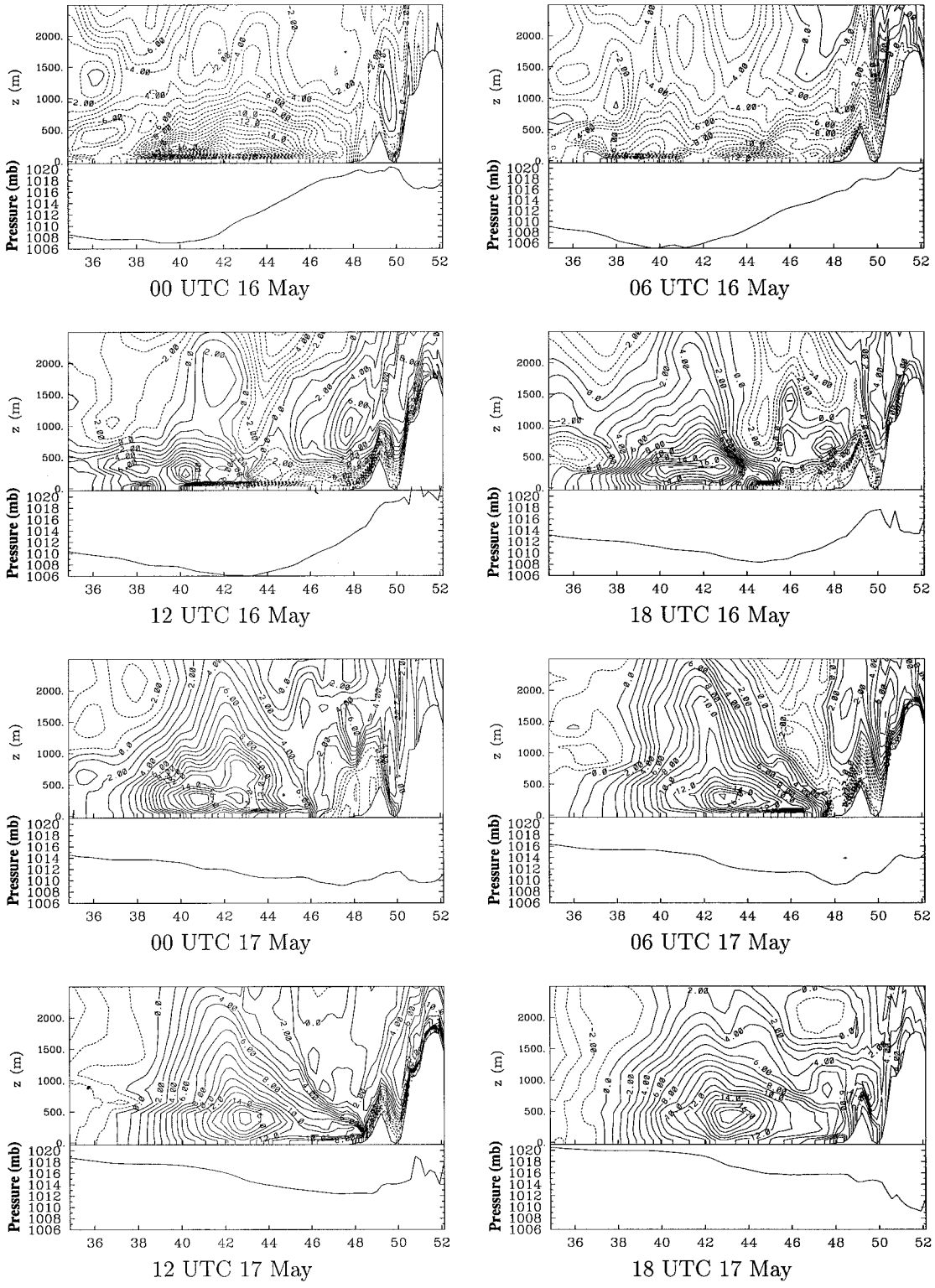

FIG. 5. Simulated south–north vertical cross sections of meridional wind speed (contour interval, 1 m s^{-1}) and sea level pressure (hPa) from grid 2 of the model during the propagation of the May 1985 CTD. The cross section is located just offshore of the northern California to Washington coasts and extends from offshore of Point Conception in the south to north of Vancouver Island in the north. Numbers along the horizontal axis indicate the latitude.

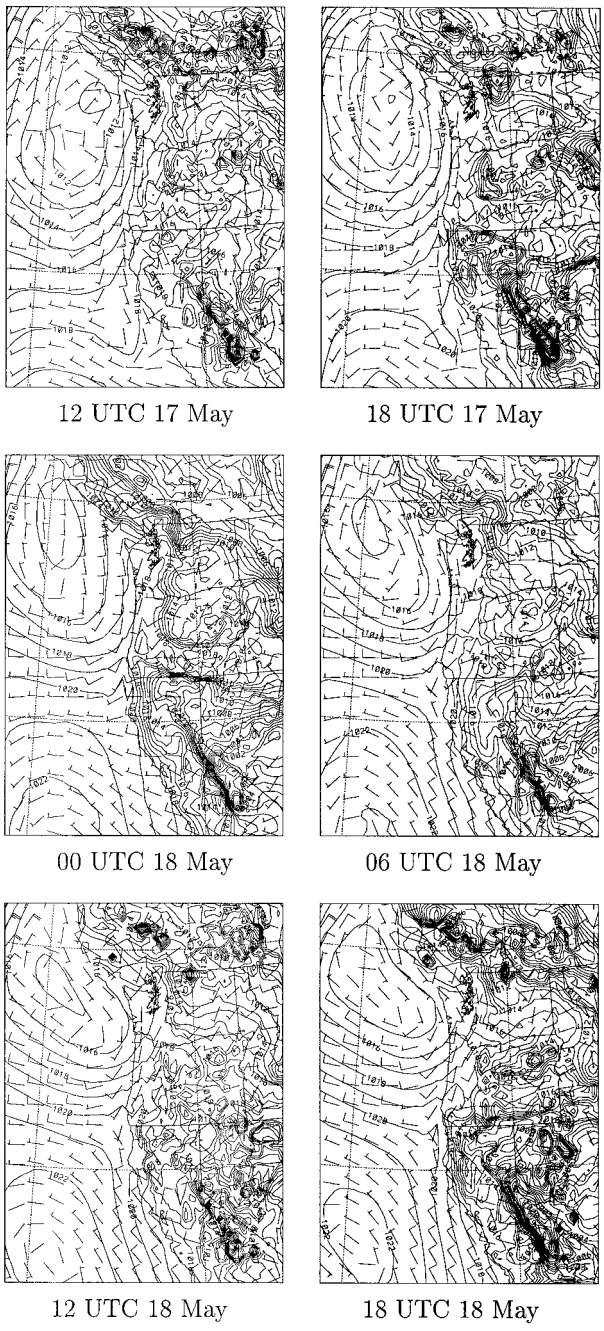

FIG. 6. Sea level pressure (contour interval, 1 mb) and wind fields at 118-m elevation during the decay of the May 1985 event from grid 2 of the northern run.

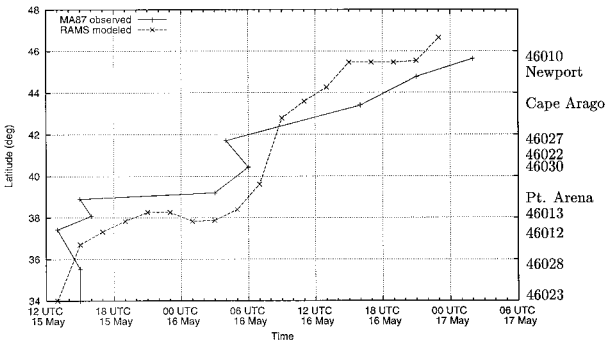

FIG. 7. The observed (solid line, from MA87) and grid 2 simulated (dashed line) position of the southerly transitions as a function of time.

west coast. However, by this time the meridional temperature (and pressure) gradient had started to weaken as the synoptic low moved farther westward and the offshore flow ahead of the CTD, and to lesser extent the onshore flow to the south that was feeding the gravity current–like flow, decreased (Fig. 6). The importance of the offshore flow ahead of the CTD for setting up the northward-directed potential temperature gradient can be seen in Fig. 2 for 0000 UTC 17 May–0000 UTC 19 May where, coincident with the weakening of the event, the boundary layer potential temperature in the north decreased much more rapidly than it increased in the south. In other words, the weakening of the event appeared to be related more to the return of the low-level potential temperature field in the north back toward preevent values, thereby weakening the northward-directed density gradient, rather than to changes in this field along the southern coast.

At 0000 UTC 18 May, the gravity current–like signature in the potential temperature field was still evident all the way north to Vancouver Island; however, the zone of southerly winds on the coast south of about the California–Oregon border had already shifted to westerly to northwesterly (Fig. 6) as the event began decaying. The last two panels for 1200 UTC 18 May and 0000 UTC 19 May (Fig. 2) show the decay of the gravity current–like signature in the potential temperature along the coast as the coastal winds switched around to westerly and then northwesterly along the coast (Fig. 6). Plots of meridional velocity near the surface (not shown) indicate that the decaying coastal zone of southerlies off Vancouver Island extended offshore in an anvil-type feature from 0000 UTC 18 to 0000 UTC 19 May, reminiscent of the shape of the leading edge of the stratus cloud bank visible in satellite imagery (MA87) of this event.

GJR98 presented plots of the timing of the southerly wind transition along the coast and the evolution of the surface pressure signal at various coastal stations, finding qualitative agreement with the observations of MA87. Similar timing of the southerly wind transition was also found for the current simulation, except that the switch along the central Californian coast was slightly closer to MA87 than was the GJR98 simulation (Fig. 7). MA87 have also calculated a speed of propagation of the event up the coast based on both the observed timing of the wind switch and the empirical gravity current formula of Seitter and Muench (1985):

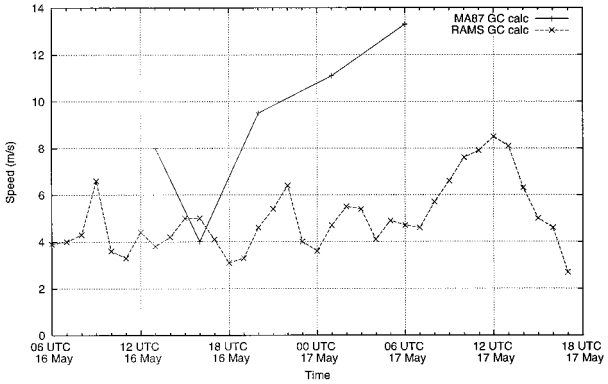

FIG. 8. Gravity current calculated speeds based on observations (solid line, from MA87) and RAMS output (dashed line).

$$V = 0.79\left(\frac{\Delta p}{\rho}\right)^{0.5},$$

where V is the gravity current propagation speed, Δp the pressure difference associated with the gravity current head (computed as the surface pressure difference between the average pressure 2 h after the arrival of the leading edge minus that of the preceding hour), and ρ is the density of the ambient air.

Data for the coastal section from the California–Oregon border to Quillayute in northern Washington (1300 UTC 16 May–0600 UTC 17 May) indicated that the event propagated at a speed of around 4–7 m s^{-1} in southern and central Oregon, and this speed increased to 10–13 m s^{-1} in northern Oregon and Washington (MA87). Reasonable agreement was found between the empirical gravity current speed and that based on the timing of the wind transition except in southern Oregon, where the CTD appeared to jump northward (MA87) and the empirical gravity current speed gave a significant underestimate. Hourly resolution surface pressure and meridional wind were extracted from the model run and used to compute a propagation speed based on both the timing of the wind transition and on the Seitter and Muench (1985) formula. Although the latter was generally slower than the MA87 calculations (Fig. 8), there was an increase in speed as the event progressed (i.e., on 17 May). Once the model event approached Vancouver Island and began to weaken (after 1200 UTC 17 May), the computed speed decreased (Fig. 8). In calculating the gravity current speed from RAMS output, an average density of 1.17 kg m^{-3} corresponding to an ambient temperature of 25°C was used. MA87 do not report the density used in their calculations, but when it is calculated from the reported Δp and plotted speeds it is found to vary between 1.0 and 1.77 kg m^{-3}. Only five surface stations (buoy 46027, northern California; Cape Arago, Oregon; Newport, Oregon; Astoria, Oregon; Quillayute, Washington) were available to calculate the speeds along the northern California to northern Washington coast derived in MA87. With these limitations, the MA87 calculations were the best that could be done, but may not give very accurate gravity current speed estimations. Another reason RAMS calculated gravity current speeds are different, and generally lower than the MA87 calculated gravity current speeds, is that the simulated gradients near the transition zone are less sharp than observed, leading to a smaller Δp in the Seitter and Muench formula. On the other hand the speed calculated on the basis of the timing of the model wind transition along the coast was highly variable, ranging from less than 4 m s^{-1} to about 17 m s^{-1}. Such variability in propagation is certainly characteristic of the generally unsteady, spurting advance of a gravity current. MA87 note an example of such behavior in the observed event, namely the jump forward of the CTD at around 0500 UTC 16 May when the leading edge was approaching buoy 46027 just south of the California–Oregon border. Were more closely spaced surface stations available, variability in the propagation of the observed event more similar to that in the model may have been observed by MA87.

"Force balance" analysis and comparison with theory

As was done for the initiation stage of the event, the "force balance" capability of RAMS is invoked to determine the relative contributions of the various terms to the meridional wind. Figure 9, showing the tendencies of meridional wind at 118-m elevation at 0000 UTC 17 May when the southerly wind transition had reached northern Oregon (about 45°–46°N), indicates that both the pressure gradient and Coriolis terms were important. The larger magnitude of the former, relative to Coriolis, in the south together with the contribution of the advective term leads to the positive tendency of the meridional wind along, and offshore of, the central California to Vancouver Island coasts and, hence, the southerly winds there. The maximum in the total meridional wind tendency can be seen to be located somewhat offshore from the California–Oregon border, near where the pressure gradient tendency is greatest (Fig. 9). A secondary maximum in total v tendency, which results from the Coriolis term, is located just ahead of the CTD. Here, offshore flow (e.g., Fig. 10) increasing away from the coast ahead of the CTD results in increased positive southerly Coriolis tendency and, hence, enhances northward propagation of the CTD.

Consistent with the semigeostrophic theory of CTDs (Reason and Steyn 1992; Reason 1994) only the across-mountain pressure gradient is geostrophically balanced, and advective and frictional effects contribute (though to lesser extent) along with the pressure gradient and Coriolis terms to the along-mountain wind. Note that the along-mountain direction considered in this theory is only slightly offset from the meridional orientation for the region between about 39° and 48°N, which is of most interest here. In this theory, a fundamental re-

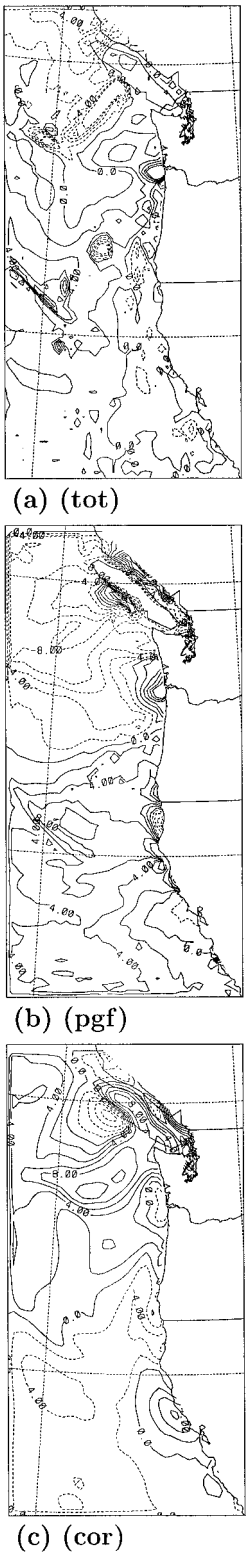

FIG. 9. Tendencies of meridional wind at 118-m elevation at 0000 UTC 17 May: (a) tot resulting from the sum of the other four tendencies, (b) tendency due to pgf, and (c) tendency due to cor. Contours are labeled in units of 10^{-4} m s^{-2} with a contour interval of 2×10^{-4} m s^{-2}.

quirement is that the length scale of the CTDs offshore from the mountains be small compared to that for the along-mountain direction. The latter may be estimated from a contour plot of the meridional wind speed (Fig. 10) for 0000 UTC 17 May, at which time the main body of the southerly wind transition had reached the northern Oregon coast (about 45°–46°N) and was south of significant gaps in the coastal mountains such as the Columbia River mouth and the Juan de Fuca Strait where CTDs sometimes slow, or even stall (e.g., Reason and Dunkley 1993). Thus, a representative scale width R for the zone of coastal southerly winds at 39°–41°N behind the leading edge of the transition can be estimated as 200 km (MA87 provide an observational estimate of 168–178 km), small compared to the approximately 1400-km meridional extent of southerly winds (scale L) at this time (30°–44°N), and consistent with expectations from the semigeostrophic theory of CTDs (Reason and Steyn 1992).

Under the assumption that the stratification can be approximated by a two-layer fluid, the semigeostrophic scaling for propagating CTDs (Reason 1994) suggests that both the across-mountain Rossby number and the parameter R/fLT (T a typical timescale, taken as 1 day here—the approximate time elapsed at 0000 UTC 17 May since the beginning of the transition to southerly winds along the coast) should be small in order for there to be an approximate geostrophic balance between the along-mountain wind and the pressure gradient in the across-mountain direction. Using the previously estimated scales for R and L, and $T = 1$ day, gives $R/fLT = 0.018$, which is small compared to unity. Taking an along-mountain velocity scale V from Fig. 10 to be 5–10 m s^{-1}, and these previously estimated R and L scales, yields an across-mountain Rossby number V/fL of 0.04–0.08, indeed small compared to unity. The along-mountain Rossby number is estimated from V/fR to be 0.27–0.54, considerably larger than the across-mountain Rossby number as required, but relatively small compared to unity. This value therefore suggests that, as expected from Fig. 9, the pressure gradient and Coriolis terms are the most important for the meridional wind tendency, with advection and friction making fairly small, though not insignificant, contributions.

Also, as expected from the theory, the strongest along-mountain winds occur in a narrow zone near the coast and decay farther offshore. The form of the decay in Fig. 10 is not exponential, as would be the case for a generic Kelvin wave under the assumption that the wave displacement vanishes far offshore. Rather, it appears that the decay of meridional wind speed is more hyperbolic in nature, with weaker decay near the coastal mountains, more rapid decay farther offshore, and then weaker decay near the boundary of the southerly CTD winds and the ambient flow. Such a situation is more consistent with the gravity current–like nature of this event, where an offshore density front is expected to separate the CTD flow from the ambient atmosphere,

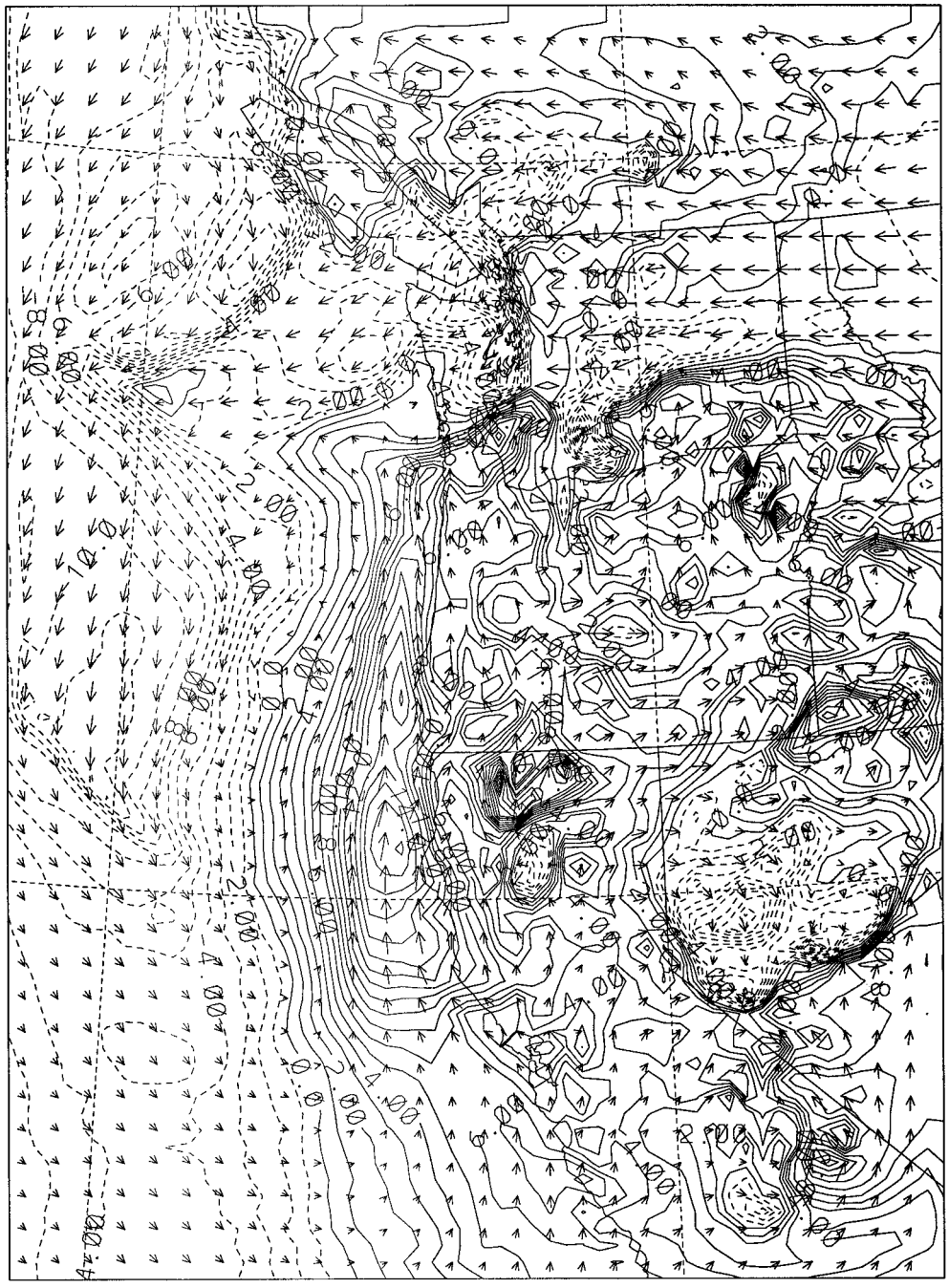

FIG. 10. Wind field at 118-m elevation at 0000 UTC 17 May. Every second wind vector in both dimensions is plotted. Contour is for meridional wind speed and the interval is 1 m s^{-1}. Dashed contours indicate winds with a northerly component; solid contours winds with a southerly component.

and the decay of the winds away from the coastal mountains is not exponential but hyperbolic (Reason and Steyn 1992).

Thus, the characteristics of the scales of the model CTD, its signature in the model temperature, sea level pressure and meridional wind fields, and the input of cool, dense air into the initiation region of the CTD (source of any gravity current–like flow) by the synoptic forcing all suggest that the event propagated northward along the coast as a gravity current–like feature trapped

against the coastal mountains. MA87 interpreted the observational record of this event to be consistent with a topographically trapped gravity current and found evidence of abrupt weather changes near the leading edge, or steep gravity current head. In the model, this steep gravity current head is not as well resolved as one would like. As discussed previously, at least part of the difficulty results from the standard NCEP fields used for model initialization not having any boundary layer structure within them.

4. CTD decay

During the decay phase, the southerly flow gradually shifts to westerly and then to northwesterly over the California coast south of about 39°–40°N (1200 UTC 17 May–0000 UTC 18 May; Fig. 6) as the synoptic low tracked farther offshore and weakened. At 1200 UTC 17 May, the flow along the coast north of San Francisco Bay was still southerly, whereas that farther south had shifted back to westerly to northwesterly. By 0000 UTC 18 May the switch to westerly to northwesterly is evident as far north as the California–Oregon border with southerlies still present to the northern tip of Vancouver Island. This situation more or less prevailed until at least 0000 UTC 19 May; that is, the flow along the coast south of southern Oregon had switched back to northwesterly whereas that to the north remained southerly.

This pattern of wind changes along the west coast as the synoptic forcing moved away and weakened resembles the decay of a gravity current flow as the input of dense fluid into the gravity current is removed, and the decaying gravity current adjusts to its environment. Thus, the decay is most noticeable near the source region and is slower to occur in the main body of gravity current fluid some distance away from the source. Consistent with this expectation, the gravity current–like signature in the potential temperature fields (Fig. 2) is still evident along the west coast of Vancouver Island at 0000 UTC 18 May whereas farther south the signal is less distinct. Over the next 24 h to 0000 UTC 19 May, the gravity current–like leading edge on the Vancouver Island coast weakened significantly as the synoptic forcing was removed.

A force balance analysis during the decay phase at 0600 UTC 18 May (Fig. 11a), some hours after the CTD had reached the northern end of Vancouver Island, indicates a small positive total tendency of meridional velocity in the region of ongoing southerly winds along the Oregon coast (main body of gravity current), and negative tendency (i.e., opposing the southerly winds) to the north (head of gravity current), consistent with the above discussion of a decaying gravity current. Weak negative total tendency, mainly driven by the Coriolis term, is also evident along the central Californian coast. In the head region along the Washington and Vancouver Island coasts, positive tendency due to Coriolis and advection is opposed by a negative contribution

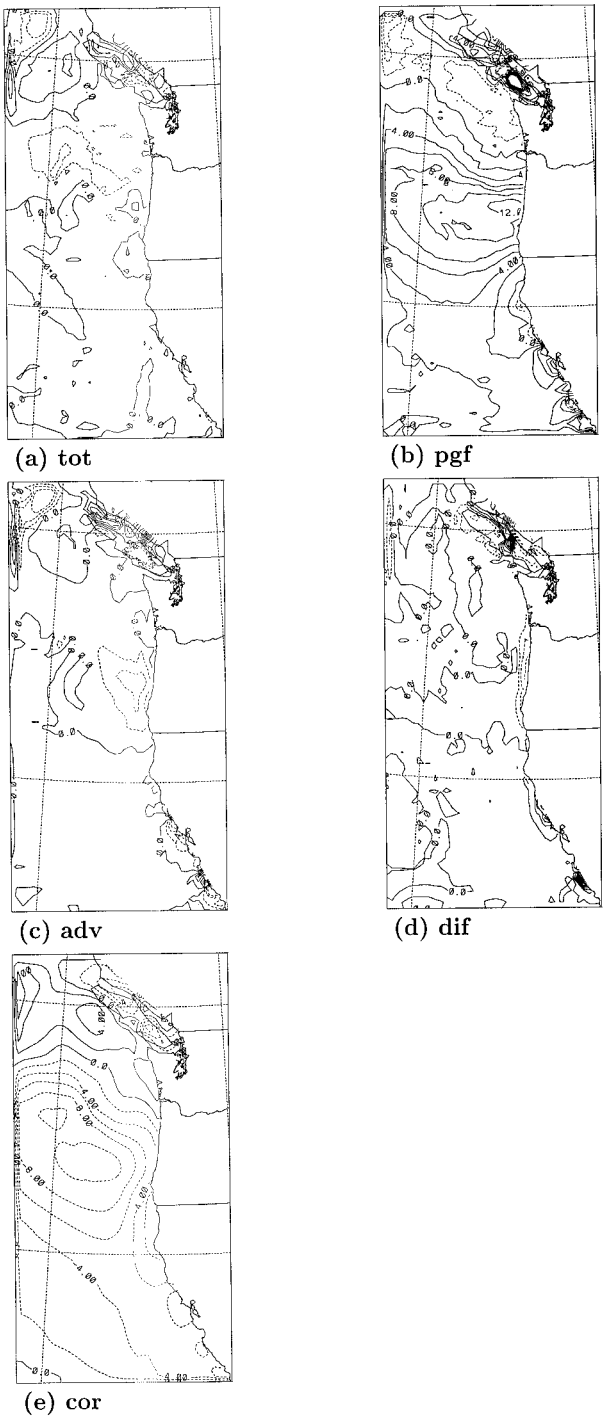

FIG. 11. Tendencies of meridional wind at 118-m elevation at 0600 UTC 18 May: (a) tot due to the sum of the following four tendencies—(b) tendency due to pgf, (c) tendency due to adv, (d) tendency due to dif, (e) tendency due to cor. Contours are labeled in units of 10^{-4} m s^{-2} with a contour interval of 2×10^{-4} m s^{-2}.

from the pressure gradient term, and to lesser extent diffusion. Farther offshore, to the southwest, a negative Coriolis term opposes any northward flow. In the region of remaining positive total tendency along the southern Oregon coast, the positive pressure gradient term is opposed by a combination of the Coriolis term and advective and diffusive deceleration of the southerly winds. By comparison to the propagation phase, it appears that advection and diffusion make a relatively large contribution in the decay phase, near both the leading edge of the CTD and farther south in the main body of southerly winds (Oregon coast).

In summary, the force balance analyses of model output for this event indicate that while the pressure gradient force resulting mostly from synoptic evolution drives the event, the contributions of the other forces in the presence of coastal orography are also important. In the initiation phase, onshore flow forced to decelerate by the coastal mountains results in a decrease in the Coriolis force leading to southerly flow. In the propagation phase, accelerating offshore flow ahead of the CTD resulted in a southerly tendency, which enhanced northward propagation of the disturbance. In the decay phase, there is a different force balance near the leading edge of the CTD from that farther south in the main body of southerly winds. Near the leading edge, the pressure gradient now opposes farther northward propagation, which is driven by the Coriolis and advective terms. Diffusion also acts to decelerate the southerly winds here. Farther south in the main body of the southerly winds (Oregon coast), the continuing strong northward pressure gradient is opposed by sizeable contributions from all three other tendencies in the meridional momentum equation (Coriolis, advection, diffusion).

5. Discussion and conclusions

Having validated in a previous paper (GJR98) a Colorado State University RAMS mesoscale model simulation of the May 1985 CTD event observed by MA87, the focus in this study has been to apply RAMS diagnostics to further understand the initiation, propagation, and decay of the event and associated dynamics. This particular CTD event is an example of a strong event, which had trapped gravity current–like characteristics, and for which the role of the synoptic forcing (a westward tracking synoptic low, with warm, offshore flow ahead of the CTD and cool onshore flow in the south) was particularly important. Thus, the difficulty in the model with adequately resolving the details of the marine boundary layer, which arises from the lack of this information in the NCEP initialization fields, is not as problematic for getting a reasonably good simulation as it possibly might be for those events where marine layer dynamics is the crucial factor for CTD evolution (GJR98).

The detailed analysis presented here has emphasized the important role of the warm offshore flow ahead of the CTD, and the cool onshore flow in the Southern California Bight, driven by the northwestward tracking low in the initiation, propagation, and decay stages of this particular event. During the initiation stage, this flow begins to create a northward-directed pressure gradient anomaly that is conducive to CTD propagation, and to build up the mass of cool, dense marine air in the Southern California Bight that can fuel the gravity current–like propagation of the event. The timing of the adjustment of the onshore flow in the bight to form the northward propagating CTD was found to be consistent with the theoretical scaling arguments developed in Reason (1994).

During the propagating stage, a gravity current–like signature was observed in the model potential temperature, meridional wind, and sea level pressure fields, although due to the boundary layer initialization handicap, the signature was somewhat less sharp than that observed by MA87. Force balance analysis of the RAMS fields suggested that the pressure gradient and Coriolis terms were most important for the meridional wind tendency, although the advective and diffusive terms also contributed. Application of the scale analysis of Reason (1994) indicated that the model CTD was semigeostrophic, consistent with the theory of Reason and Steyn (1992), whereby the along-mountain velocity is in geostrophic balance with the pressure gradient in the across-mountain direction whereas the along-mountain pressure gradient is not geostrophically balanced.

For this event, decay, and finally termination, was essentially caused by the removal of favorable synoptic forcing along the coastal zone. There appeared to be little or no contribution in this process from topographic effects unlike for some other CTD events along this coast or that of southeastern Australia (Reason and Steyn 1992; Reason and Dunkley 1993). These variations in the lifespan of CTD events makes their forecasting along the northern part (Washington, west coast of Vancouver Island, and sometimes beyond) of their propagation domain particularly problematic. For example, the event analyzed in Reason and Dunkley (1993) appeared to stall at the Columbia River mouth for at least 8 h before restarting, then weakening near the Strait of Juan de Fuca between Washington and Vancouver Island, and finally propagating to the northern tip of Vancouver Island.

Taken together, this study and the previous one of GJR98 suggest that the RAMS model in its current configuration can be usefully applied to these strong CTD events that are closely linked to the synoptic forcing. On that basis, a follow-on study is aimed at investigating the sensitivity of this event to surface characteristics such as the sea surface temperature and terrain elevation in order to better understand the smaller-scale aspects of CTDs and their manifestation in certain sensitive localized regions.

Acknowledgments. Support for this project came from

the U.S. Office of Naval Research Coastal Meteorology Accelerated Research Initiative Grants N00014-96-1-0745 and N00014-97-1-0342. RAMS was developed under the support of the National Science Foundation and the U.S. Army Research Office.

REFERENCES

Dorman, C. E., 1985: Evidence of Kelvin waves in California's marine layer and related eddy generation. *Mon. Wea. Rev.*, **113,** 827–839.

——, 1987: Possible role of gravity currents in northern California's marine layer and related eddy generation. *J. Geophys. Res.*, **92,** 1497–1506.

Guan, S., P. L. Jackson, and C. J. C. Reason, 1998: Numerical modeling of a coastal trapped disturbance. Part I: Comparison with observations. *Mon. Wea. Rev.*, **126,** 972–990.

Mass, C. F., and M. D. Albright, 1987: Coastal southerlies and alongshore surges of the west coast of North America: Evidence of mesoscale topographically trapped response to synoptic forcing. *Mon. Wea. Rev.*, **115,** 1707–1738.

Pierrehumbert, R. T., and B. Wyman, 1985: Upstream effects of mesoscale mountains. *J. Atmos. Sci.*, **42,** 977–1003.

Ralph, F. M., P. J. Neiman, P. O. G. Persson, W. D. Neff, J. Miletta, L. Armi, and J. M. Bane, 1995: Observations of an orographically trapped disturbance along the California coast on 10–11 June 1994. Preprints, *Seventh Conf. on Mountain Meteorology*, Breckenridge, CO, Amer. Meteor. Soc., 204–211.

Reason, C. J. C., 1994: Orographically trapped disturbances in the lower atmosphere: Scale analysis and simple models. *Meteor. Atmos. Phys.*, **53,** 131–136.

——, and D. G. Steyn, 1992: The dynamics of coastally trapped mesoscale ridges in the lower atmosphere. *J. Atmos. Sci.*, **49,** 1677–1692.

——, and R. Dunkley, 1993: Coastally trapped stratus events in British Columbia. *Atmos.–Ocean*, **31,** 235–258.

Seitter, K. L., and H. S. Muench, 1985: Observation of a cold front with rope cloud. *Mon. Wea. Rev.*, **113,** 840–848.